IEEE Access
Multidisciplinary | Rapid Review | Open Access Journal

Received 1 September 2023, accepted 4 October 2023, date of publication 12 October 2023, date of current version 18 October 2023.

Digital Object Identifier 10.1109/ACCESS.2023.3324055

APPLIED RESEARCH

Variable Leakage Flux Permanent Magnet Synchronous Machine PM Temperature Estimation Based on PM Flux Linkage

DIEGO F. LABORDA[1], (Member, IEEE), DAVID REIGOSA[1], (Senior Member, IEEE), DANIEL FERNÁNDEZ[1], (Member, IEEE), KENSUKE SASAKI[2], TAKASHI KATO[2], (Member, IEEE), AND FERNANDO BRIZ[1], (Senior Member, IEEE)

[1]Department of Electrical, Computer and Systems Engineering, University of Oviedo, 33203 Gijón, Spain
[2]EV System Laboratory, Nissan Motor Company Ltd., Atsugi, Kanagawa 243-0123, Japan

Corresponding author: Diego F. Laborda (dflaborda@uniovi.es)

This work was supported by Nissan Motor Company Ltd.

ABSTRACT The performance of Permanent Magnet Synchronous Machines (PMSMs) is significantly influenced by the temperature of the Permanent Magnets (PMs). Therefore, accurate knowledge of PM temperature is necessary for control and monitoring purposes. As temperature rises, the magnetic flux strength of PMs, and consequently the torque production capability of PMSMs, diminishes. Moreover, there is a risk of irreversible demagnetization of the PMs. In the case of Variable Leakage Flux PMSMs (VLF-PMSMs), the temperature impacts the machine's variable leakage property, potentially compromising the accuracy of torque control. The current state-of-the-art PM temperature estimation methods are unsuitable for VLF-PMSMs due to their variable leakage PM flux characteristics. This paper addresses the limitations of existing PM temperature estimation methods by incorporating the variable leakage PM flux property of VLF-PMSMs. The proposed method utilizes PM flux linkage derived from the machine's response to a small-amplitude, low-frequency, quasi-square-wave current signal. This signal is superimposed onto the fundamental excitation, enabling online temperature estimation without altering the machine's operation.

INDEX TERMS Permanent magnet, signal injection, temperature estimation, VLF-PMSMs.

I. INTRODUCTION

Permanent Magnet Synchronous Motors (PMSMs) are highly appealing for electric and hybrid-electric vehicles (EV & HEV) owing to their superior torque density, wide speed range, and efficiency. However, a notable concern for these motors arises when operating at high speeds. In such cases, it becomes necessary to introduce negative d-axis current to counterbalance the flux linkage of the permanent magnets (PMs) in order to match the back electromotive force (Back-EMF) with the available DC voltage [1]. This operational mode, known as flux-weakening, increases copper and core losses due to the continuous injection of negative d-axis current and producing additional harmonics in the airgap field [1]. These supplementary losses contribute to reduced efficiency, elevated machine temperatures, and potential implications for the motor's lifespan. In order to decrease or eliminate the need for flux-weakening current injection and its subsequent adverse effects, novel machine designs such as Variable Flux PMSMs (VF-PMSMs) [2] and Variable Leakage Flux PMSMs (VLF-PMSMs) [3] have been developed. VF-PMSMs actively modify the PM magnetization level using the stator current during normal operation in order to reduce the back-EMF, and consequently reducing or even avoiding the flux weakening current injection. VLF-PMSMs use a special rotor design to passively reduce the back-EMF when the machine is operated at low load, which allows the use of lower flux weakening current at high speed while maintaining the characteristic high torque density of conventional IPMSMs at low speeds and high load.

The associate editor coordinating the review of this manuscript and approving it for publication was Feifei Bu.

Irrespective of the specific design of the PMSM, monitoring the magnets' temperature is a critical issue. The reason is that an increase in the temperature of the PMs leads to a decrease in their magnetic strength, which subsequently reduce the machine's torque production capability. Moreover, elevated temperatures can potentially cause irreversible demagnetization of the PMs.

At low-speeds, the main loss in PM machines is copper loss; while at high-speeds, the main losses are hysteresis loss and eddy current loss. Therefore, the temperature rise at low-speeds is mainly produced in the stator windings; while the temperature rise at high-speeds is mainly produced in the rotor PMs and core. The heat extraction from stator is fairly simple since it can be accomplished by means of natural convection or forced convection using e.g., air, water, or oil; however, heat extraction from the rotor is harder to accomplish due to its mechanical rotation and being surrounded by the stator which acts as a heat source. It can be concluded that, regarding PM temperature monitoring, the most critical speed-region is mid-to-high-speed region.

The dependence of PM's magnetic strength on temperature introduces additional concerns in both VF-PMSMs and VLF-PMSMs. In VF-PMSMs, variations in PM magnetic strength affect the magnetization/demagnetization process, and torque control [4]. In VLF-PMSMs, variations in PM magnetic strength directly impact the variable leakage property of the machine, potentially compromising the accuracy of torque control [5]. Thus, it becomes evident that accurate knowledge of PMs' temperature is vital for monitoring purposes and, also, for precise torque control, where the latter typically demands higher accuracy requirements [6].

Direct measurement of PM temperature in PMSMs typically involves the use of rotor-mounted sensors and slip rings or wireless transmission systems. However, these methods can compromise the system's robustness and increase costs. An alternative approach is to estimate the PM temperature.

PM temperature estimation methods can be broadly categorized into thermal models [7], [8], [9], [10], back-EMF based methods [10], [11], [12], [13], [14], and signal injection methods [15], [16], [17], [18], [19]. Thermal models rely on knowledge of the stator and rotor geometry, materials, and cooling system, making them highly dependent on the machine design [7], [8], [9], [10]. In contrast, back-EMF and signal injection methods do not require prior information about the machine's geometry and cooling system [10], [11], [12], [13], [14], [15], [16], [17], [18], [19]. However, both methods require knowledge of machine parameters such as inductance, stator resistance, and stator temperature to compensate for variations in stator resistance with temperature [10], [11], [12], [13], [14], [15], [16], [17], [18], [19]. In many cases, this is not a significant drawback as the stator winding temperature is commonly measured using contact-type sensors in standard PMSMs. Signal injection methods are applicable across the entire speed range, while back-EMF based methods are not suitable for low speeds or standstill since the back-EMF is proportional to speed. However, signal injection methods are susceptible to saturation and magnetoresistive effects [20]. Moreover, they need the injection of an additional signal, which raises concerns regarding losses, noise, vibration, and torque ripple. These limitations make back-EMF based estimation methods particularly appealing in the mid-to-high-speed region.

TABLE 1. Advantages and drawbacks of PM temperature estimation methods based on PM flux linkage.

	No need of voltage sensors	No PM flux linkage linear behavior	No need of LUTs
[10]	-	✗	✗
[11]	✗	✗	✗
[12]	✓	✗	✗
[13]	✓	✗	✗
[14]	✓	✗	✗
[21]	✗	✗	✓
Proposed method	✓	✓	✗

Back-EMF-based estimation methods rely on a linear relationship between PM flux linkage and PM temperature across the entire current range [10], [11], [12], [13], [14]. This assumption is generally valid for PMSMs, as changes in PM flux linkage with stator current are minimal in these machines. In [11], a PM temperature observer is presented, which utilizes current and voltage measurements. However, this method requires the use of look-up tables (LUTs) to establish the correlation between stator current and flux. While current sensors are commonly available in industrial drive systems, voltage sensors are not typically included, leading to increased system costs. To address this limitation, [12] proposes using the current controller command instead of voltage sensors. Additionally, this method considers the impact of airgap length variation caused by the thermal expansion of the stator and rotor. Another approach is presented in [13], where a Kalman filter with a linear state-space model and LUTs is utilized for estimation. This method combines the advantages of the Kalman filter for state estimation with LUTs for improved accuracy. In [10], the range of estimation is extended to low speeds and standstill by incorporating a thermal model based on a particle swarm optimization commissioning. In [21], high bandwidth measurements of PWM voltage and current waveforms are employed for PM flux linkage and temperature estimation. However, this method is less suitable for interior PMSMs, as it becomes sensitive to machine inductance when there is d-axis current. Table 1 summarizes the major advantages and limitations of back-EMF-based estimation methods.

Applying existing PM temperature estimation methods to VLF-PMSMs result in significant estimation errors due to their notable variations in inductances and PM flux linkage with stator current [2]. In conventional PMSMs, the PM flux linkage is fairly constant with q-axis (load) current; while in VLF-PMSMs, the PM flux linkage is reduced at low q-axis current magnitudes. The behavior of VLF-PMSMs' PM flux

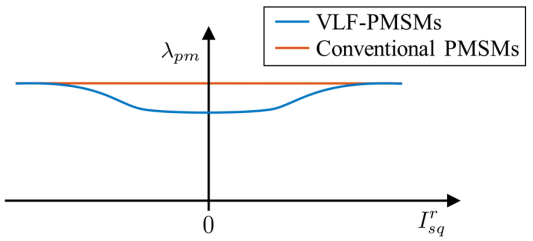

FIGURE 1. PM flux linkage vs. q-axis current of a VLF-PMSM and an equivalent conventional PMSM.

linkage with q-axis current is represented in Fig. 1 along with an equivalent conventional PMSM PM flux linkage for comparison.

Due to this variation of PM flux linkage with stator current, the PM flux linkage cannot be directly related to PM temperature (i.e., already proposed methods in the literature [10], [11], [12], [13], [14], [21]) in this type of machines. Therefore, a method considering the variable PM flux linkage of VLF-PMSMs is proposed in this paper.

In [22], these limitations are addressed by injecting a small-amplitude, low-frequency, quasi-square-wave current signal on top of the fundamental excitation to estimate the PM flux linkage. However, the method proposed in [22] does not consider magnetic saturation of the d-axis, resulting in large estimation errors in the d-axis inductance and PM flux linkage. Additionally, [22] provided very limited experimental validation of the method in the torque vs. speed region and during torque and speed transients, which are critical to demonstrate the effectiveness of the method in EVs and HEVs applications.

This paper addresses all these limitations by:

- Improving the PM flux linkage estimation considering the magnetic saturation of d-axis using the small-amplitude, low-frequency, quasi-square-wave current signal.
- Proposing a method to estimate the DC inductance from dynamic inductance.
- Providing experimental verification of the method in the whole torque vs. speed region.
- Providing experimental verification of the method during torque and speed transients demonstrating the effectiveness of the method in EVs and HEVs applications.

This paper is organized as follows: principles and implementation of the proposed temperature estimation method are presented in Section II; simulation results are provided in Section III; Section IV shows the experimental results; Section V concludes the paper.

II. PM TEMPERATURE ESTIMATION BASED ON PM FLUX LINKAGE VARIATION

This section provides an overview of the principles and implementation details of the proposed temperature estimation method.

As previously mentioned, it is well-established that there is a decrease in PM flux linkage as the PM temperature

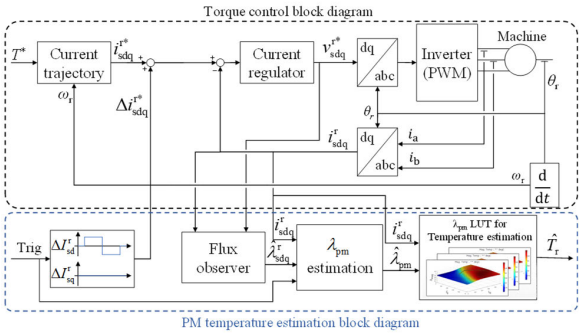

FIGURE 2. Temperature estimation system scheme.

increases [10], [11], [12], [13], [14], [15], [16], [17], [18], [19], [20], [21], [22], [23], [24]. Therefore, PM flux linkage serves as a reliable metric for estimating PM temperature.

The d- and q-axis flux linkages can be modeled as:

$$\lambda^r_{\mathrm{sd}} = i^r_{\mathrm{sd}} L_d + \lambda_{\mathrm{pm}}, \tag{1}$$

$$\lambda^r_{\mathrm{sq}} = i^r_{\mathrm{sq}} L_q, \tag{2}$$

where λ^r_{sd} and λ^r_{sq} are the stator d- and q-axis flux linkages in the rotor synchronous reference frame, L_{d} and L_{q} are the d- and q-axis stator inductances, λ_{pm} is the PM flux linkage, and i^r_{sd} and i^r_{sq} are the stator d- and q-axis currents, respectively.

Alternatively, they can be modelled as function of d- and q-axis stator voltages, currents, and stator resistance, R_s, as:

$$\lambda^s_{\mathrm{sd}} = \int (v^s_{\mathrm{sd}} - R_s \cdot i^s_{\mathrm{sd}}) \cdot dt, \tag{3}$$

$$\lambda^s_{\mathrm{sq}} = \int (v^s_{\mathrm{sq}} - R_s \cdot i^s_{sq}) \cdot dt. \tag{4}$$

where λ^s_{sd} and λ^s_{sq} are d- and q-axis flux linkages, i^s_{sd} and i^s_{sq} are the d- and q-axis stator currents, and v^s_{sd} and v^s_{sq} are the d- and q-axis stator voltage in the stationary reference frame.

It can be concluded from (1) that L_{d} and λ_{pm} can be obtained from λ^s_{sd} by slightly modifying the d-axis current I^r_{sd} value. In this paper, λ_{pm} will be estimated using (1) with the small amplitude, low-frequency, quasi-square-wave current injection proposed in [5]. A flux observer based on (3)-(4) is used to estimate λ^r_{sd} while the quasi-square-wave signal is applied.

The proposed PM temperature estimation is integrated in the torque/current control block diagram of a VLF-PMSMs as shown in Fig. 2, the main blocks being:

- Flux observer: used to estimate the stator flux linkage ($\hat{\lambda}^r_{\mathrm{sdq}}$) using (3)-(4).
- PM flux linkage estimator: $\hat{\lambda}_{\mathrm{pm}}$ is estimated from $\hat{\lambda}^r_{\mathrm{sdq}}$ by the response of the machine to the small-amplitude, low frequency, quasi-square-wave current injected on top of the fundamental current ($\Delta i^{r*}_{\mathrm{sdq}}$) [5], [22].
- Temperature estimation Look-up table (LUT): linking the PM temperature with $\hat{\lambda}_{\mathrm{pm}}$ considering its variation with stator current.

It is also noted that the total d-axis stator flux could be used to estimate the PM temperature instead of PM flux

TABLE 2. Advantages and drawbacks of flux models.

	CURRENT MODEL	VOLTAGE MODEL	GOPINATH
Low parameter sensitivity at high speed	✗	✓	✓
Estimation in the whole speed range, including standstill	✓	✗	✓

linkage, avoiding the need of using the method proposed in [5]. However, the variation of the magnetic permeability due to temperature on ferromagnetic materials [25] requires including the stator temperature as an additional dimension in the total d-axis stator LUT. Due to the limitations on the computational burden and memory size present in industrial drives, the LUT based on the PM flux linkage and the method proposed in [5] are considered the most beneficial option and is used in this paper.

All the blocks shown in Fig. 2 used for PM temperature estimation are described in detail following:

A. FLUX OBSERVER

In order to estimate the stator flux, several observers are available in the literature. These observers can be categorized into different types such as those based on the voltage model (3)-(4) [26], [27], on the current model (1)-(2) [28], and Gopinath type flux observers [26].

The current model offers the advantage of estimating the stator flux across the entire speed range of the machine. However, it requires prior knowledge of parameters such as PM flux linkage and inductances, making it not viable for PM flux linkage estimation.

On the other hand, the voltage model can effectively estimate the machine's stator flux at high speeds [26]. However, its accuracy diminishes at low speeds due to the decreasing magnitude of the Back-EMF with speed. Additionally, estimating the flux using a pure integrator introduces an initial estimation error in the form of an integration constant, which must be canceled [26], [29].

The Gopinath type flux observer, as described in [26], combines the voltage model (suitable for high speeds) and the current model (suitable for low speeds, including standstill) by incorporating a PI controller to ensure a smooth transition between the two models. The bandwidth of the controller determines the frequency at which the transition from the current model to the voltage model occurs. This integrated observer provides reliable flux estimation throughout the entire speed range, including standstill. It is worth noting that the Gopinath-type observer is more sensitive to machine parameters (i.e. PM flux linkage, stator resistance and, machine inductances) at low speeds due to its dependence on the current model and the reduced magnitude of the Back-EMF. Table 2 summarizes the advantages and limitations of the three models.

In conclusion, based on the preceding analysis, it is evident that the current model and Gopinath-type flux observers, while suitable for the entire speed range of the machine, do not offer the capability to estimate the PM flux linkage.

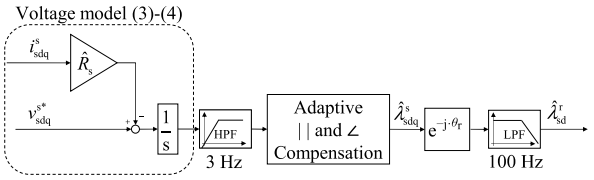

FIGURE 3. Voltage model flux observer in stationary reference frame.

This limitation arises from the fact that the PM flux linkage is an input parameter in the current model equations (1)-(2), rendering them unsuitable for PM flux linkage estimation. Consequently, this paper will employ a voltage model flux observer (3)-(4) in the stationary reference frame for stator flux estimation.

The implementation of the voltage model-based flux observer (3)-(4) is illustrated in Fig. 3. Instead of directly measuring voltages, the voltage command of the current regulator is utilized, taking into account inverter nonlinearities caused by the PWM dead time [30]. To compensate for the stator resistance voltage drop, the measured resistance at 20 °C and the stator temperature measured by thermocouples are employed. The estimated stator flux linkage in the stationary reference frame, λ^s_{sdq}, is derived from (3)-(4) after applying a 3 Hz first order high-pass filter (HPF) to avoid infinite DC gain associated with pure integration [31]. For rotor electrical speeds larger than 300 Hz the effect of the HPF in the magnitude and phase of the fundamental component is negligible. For rotor electrical speeds between 30 Hz and 300 Hz, there is a small (but not negligible) phase shift and magnitude attenuation. In order to compensate the phase shift and attenuation, an adaptive compensation, dependent on the electrical speed, is employed. This observer is not intended to be used below 30 Hz of electrical speed (5% of maximum speed) due to the diminishing magnitude of the Back-EMF.

To obtain the estimated stator flux linkage in the rotor reference frame, λ^r_{sdq}, Park's transformation is applied. Lastly, a 100 Hz first-order low-pass filter (LPF) is employed to eliminate high-frequency harmonics in the stator flux linkage, such as the 6^{th} and 12^{th} harmonics. Consequently, only the fundamental component of the stator flux linkage is utilized for temperature estimation. In this paper, a 100 Hz cutoff frequency LPF is used for the operating conditions that will be shown in simulation and experimental results. However, if the machine is operated at lower speeds (below 5% of maximum speed), the bandwidth of this filter should be modified accordingly. An adaptive cutoff frequency of the LPF might be required based on machine speed since these harmonics are produced at multiples of the machine fundamental frequency. Note that this LPF is implemented in the rotor synchronous reference frame, meaning that the fundamental component of the stator flux linkage is a DC component. Therefore, there is no phase-shift or magnitude attenuation of the fundamental component at any speed or cutoff frequency. However, the tracking of dynamic changes in the stator flux linkage (by PM temperature or stator current)

could be affected by the LPF. While this could be an issue for stator flux linkage observers used for purposes requiring high bandwidth, such as torque estimation, this is not an issue for the proposed PM temperature estimation method since the PM temperature varies very slowly compared to the stator flux linkage due to the thermal inertia of the rotor.

This voltage model flux observer (see Fig. 3) provides accurate stator flux estimation from mid-to-high speed. However, it decreases its accuracy in the low-to-zero-speed region due to the Back-EMF magnitude reduction with decreasing speed. Nevertheless, this issue is minor since, as previously discussed, the most important speed-region for PM temperature estimation is the mid-to-high-speed region. Additionally, if estimation at very low and zero speeds is mandatory, the proposed estimation method can be combined with other estimation methods already proposed in the literature that provide good accuracy in the low-to-zero-speed region [7], [8], [9], [10], [15], [16], [17], [18], [19], achieving PM temperature estimation in the whole speed range.

B. PM FLUX LINKAGE ESTIMATION

The saturation effect should be considered for PM flux linkage estimation since it has a large variation with stator currents.

In this paper, the PM flux linkage estimation method proposed in [22] is enhanced. Reference [22] uses the dynamic inductance instead of the DC inductance, resulting therefore in PM flux linkage estimation errors. Nevertheless, it is possible to obtain the DC inductance considering magnetic saturation from the dynamic inductance by (5) and (6) [32], [33]:

$$L_{dDC} = \frac{\int L_{dDyn} di^r_{sd}}{I^r_{sd}}, \tag{5}$$

$$L_{qDC} = \frac{\int L_{qDyn} di^r_{sq}}{I^r_{sq}}. \tag{6}$$

where, L_{dDyn} is the d-axis dynamic inductance and L_{qDyn} is the q-axis dynamic inductance, obtained by injecting a low frequency, low amplitude quasi-square-wave current [22], L_{dDC} is the d-axis DC inductance and L_{qDC} is the q-axis DC inductance. However, this methodology could result in large estimation errors due to integration drift.

Integration can be discretized by using the forward Euler approximation as follows:

$$L_{dDC} = \frac{\sum_{k=1}^{n} L_{dDyn}(k)\, \Delta I^r_{sd}}{I^r_{sd}}, \tag{7}$$

$$L_{qDC} = \frac{\sum_{k=1}^{n} L_{qDyn}(k)\, \Delta I^r_{sq}}{I^r_{sq}}. \tag{8}$$

where ΔI^r_{sd} and ΔI^r_{sq} are the increments of d and q-axis fundamental current between two measured dynamic inductance values, and $n = I^r_{sd}/\Delta I^r_{sd}$ (or $n = I^r_{sq}/\Delta I^r_{sq}$) is the number of current increments.

Therefore, the integration drift issue can be overcome by selecting a constant current increment ΔI^r_{sd} (and ΔI^r_{sq}) and rearranging (7) and (8) as:

$$L_{dDC} = \frac{\sum_{k=1}^{n} L_{dDyn}(k)}{n}, \tag{9}$$

$$L_{qDC} = \frac{\sum_{k=1}^{n} L_{qDyn}(k)}{n}. \tag{10}$$

From (9) and (10), it is shown that the DC inductance can be estimated by computing the mean value of dynamic inductances from zero fundamental current.

In order to demonstrate the effectiveness of the proposed method, the q-axis dynamic inductance (L_{qDyn}) is estimated using the low-frequency small amplitude quasi-square-wave current signal injection on top of the fundamental q-axis current [22]. The estimated q-axis DC inductance ($\hat{L}_{qDC}$) is obtained by computation of (10), i.e. the mean value of L_{qDyn}. The q-axis DC inductance (L_{qDC}) is obtained as λ^r_{sq}/I^r_{sq} to verify the estimation method precision. In Fig. 4, L_{qDyn}, L_{qDC} and $\hat{L}_{qDC}$ are shown. Slight differences between L_{qDC} and $\hat{L}_{qDC}$ due to the integral discretization method and the current increment step magnitude ($\Delta I^r_{sq} = 50$A) can be observed; note that differences between L_{qDC} and $\hat{L}_{qDC}$ can be reduced by decreasing ΔI^r_{sq}.

Finally, the PM flux linkage can be obtained considering magnetic saturation of d-axis due to both d and q-axis stator currents using (1).

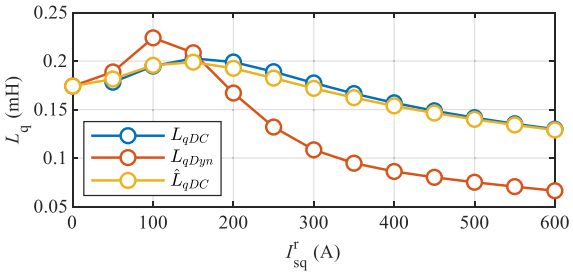

FIGURE 4. FEA results. q-axis inductance vs q-axis current. $\omega_r = 3750$ 1/min.

C. TEMPERATURE ESTIMATION

The estimation of PM temperature using PM flux linkage poses significant challenges in VLF-PMSMs, primarily due to the dependency of PM flux linkage on the stator current. To address this challenge, LUTs will be employed to compensate for the effect of current on PM flux linkage [5]. These LUTs will be constructed by storing the estimated PM flux linkage ($\hat{\lambda}_{\text{pm}}$) values corresponding to various currents and PM temperatures.

Fig. 5 shows the LUT obtained from FEA using the proposed method in Section II-B for the VLF-PMSMs test machine that will be used for the experimental verification. Fig. 5 shows the correlation between PM flux linkage and PM temperature (T_{r}). A significant decrease in PM flux linkage can be observed as the PM temperature rises. Additionally, the graph showcases the pronounced impact of q-axis current on PM flux linkage, exhibiting the expected behavior of VLF-PMSMs [5]. This observation emphasizes the crucial

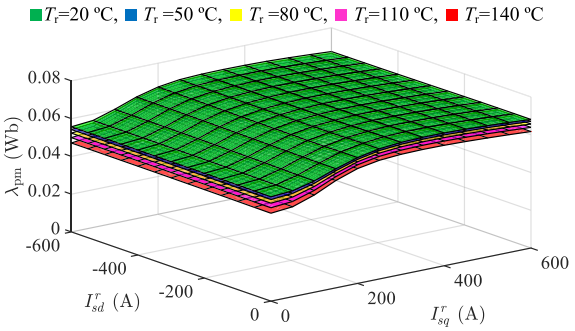

FIGURE 5. FEA results. PM flux linkage vs. stator current and PM temperature LUTs. $\omega_r = 3750$ 1/min, $T_r = 20, 50, 80, 110$ and 140 °C.

TABLE 3. Machine parameters.

P_{Rated} (kW)	I_{Rated} (A)	ω_r (1/min)	T_{Rated} (Nm)	*Poles*	Magnet type
110	640	10000	250	8	NdFeB

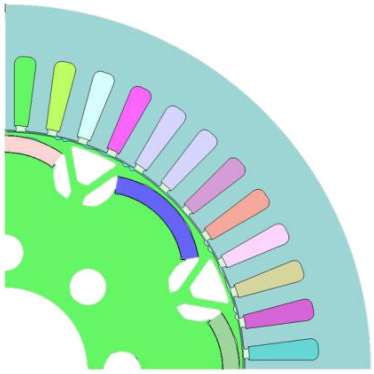

FIGURE 6. Schematic representation of the test machine.

consideration of stator current influence when implementing PM temperature estimation in VLF-PMSMs.

III. SIMULATION RESULTS

The VLF-PMSM chosen for the simulation and experimental validation of the proposed method is represented in Fig. 6. Detailed specifications and parameters of the machine can be found in Table 3.

The results are shown only for positive q-axis current since the behavior of the machine is symmetric, i.e the variation of PM flux linkage (variable leakage flux property) with q-axis current is symmetrical and only depends on the magnitude of the q-axis current (see Fig. 1).

Fig. 7a and Fig. 7b show the d- and q-axis currents, respectively where the quasi-square-wave current injected on top of the fundamental d-axis current can be observed. The magnitude of the injected signal is $|\Delta I^r_{\text{sd}}| = 8.2$ A (0.013 pu). In Fig. 7c and Fig. 7d, the estimated stator d-axis and q-axis flux linkages are depicted using the flux observer described in Section II, respectively. The estimation results are shown for five different PM temperatures.

After the PM flux linkage is estimated from (1) using the d-axis DC inductance estimated by the method described in Section II-B, it is used as an input to LUTs, from which temperature is estimated. Note that a 3D interpolation must be

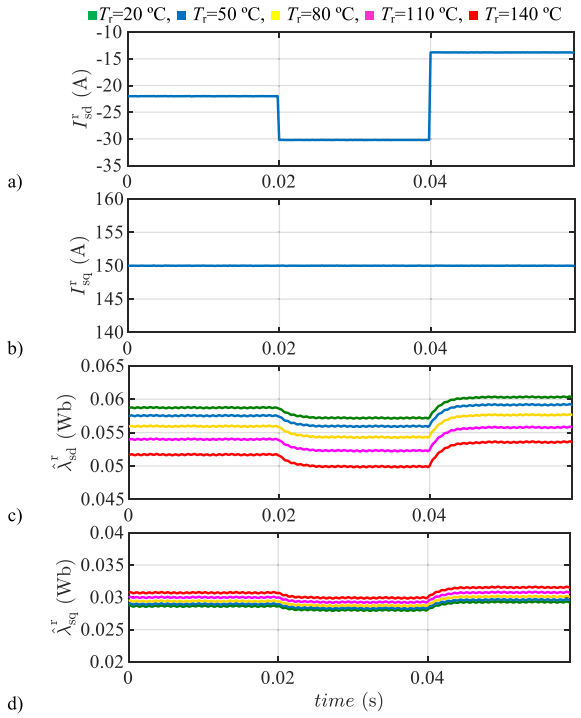

FIGURE 7. FEA results. a) d-axis and b) q-axis current c) estimated d-axis stator flux linkage and d) estimated q-axis stator flux linkage. $I^r_{sd} = -22A$, $I^r_{sq} = 150A$, $\omega_r = 3000$ 1/min, $T = 50$ Nm, $T_r = 20, 50, 80, 110$ and 140 °C.

performed during normal operation of the machine since the operating point might not meet with LUT collected values.

To perform 3D interpolation, the process involves three sequential steps: (i) interpolation through the d-axis current, (ii) interpolation through the q-axis current, and (iii) interpolation through the PM flux linkage axis. The first two interpolations are employed to predict the PM flux linkage at pre-determined temperatures (20, 50, 80, 110, 140 °C) based on the actual current. Subsequently, the PM temperature can be estimated by interpolating between the predicted PM flux linkage (obtained from steps (i) and (ii)) and the estimated PM flux linkage. Three different interpolation methods have been evaluated: linear interpolation, cubic spline interpolation and, a combination of linear interpolation for d- and q-axis with quadratic regression for PM flux linkage axis.

In Fig. 8, the temperature estimation error arising from the three interpolation methods is presented. Cubic spline interpolation shows the lower estimation error. On the other hand, the linear interpolation method exhibits larger errors in temperature estimation. Quadratic regression shows an slight increase in estimation error compared to cubic spline interpolation but with lower computational burden. For final temperature estimation results, linear interpolation will be used in this paper as it provides the lowest computational time and memory size. In scenarios where the execution time, computational cost, and memory requirements are not determining factors, spline interpolations could be more appealing.

Finally, Fig. 9 represents the PM temperature estimation error of the proposed method employing LUT linear interpolations. Estimation error is shown to be within 10 °C.

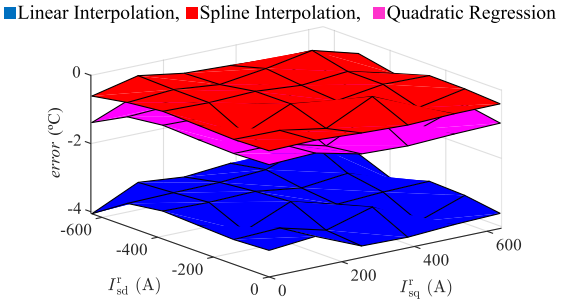

FIGURE 8. FEA results. Introduced temperature estimation error by PM flux interpolations vs. stator current at T_r = 80 °C and ω_r = 3750 1/min.

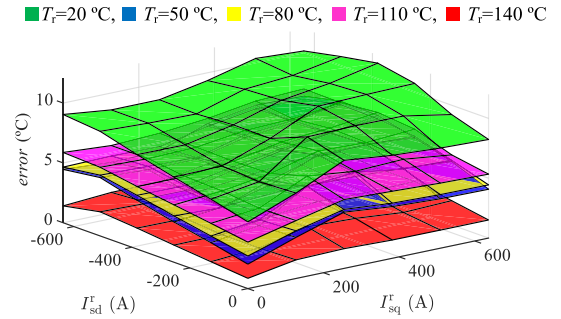

FIGURE 9. FEA results. Temperature estimation error. ω_r = 3750 1/min, T_r = 20, 50, 80, 110 and 140 °C.

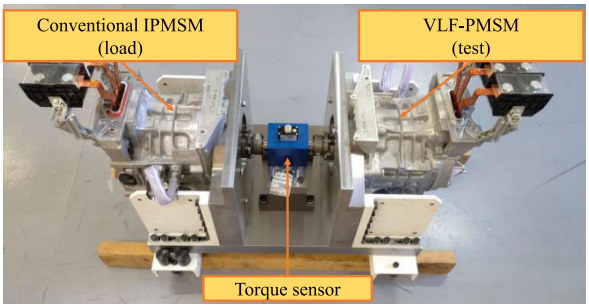

FIGURE 10. Test bench.

IV. EXPERIMENTAL SETUP AND RESULTS

A. EXPERIMENTAL SETUP

Fig. 10 illustrates the test bench employed for the experimental verification of the proposed method. The test bench consists of one IPMSM utilized as load and the VLF-PMSM under examination (parameters can be found in Table 3). Both machines are driven by separate three-phase inverters connected by the DC-link, and are controlled using a TMS320F28335 microcontroller. Finally, the PCBs used for machine control and auxiliary components are shown in Fig. 11.

The proposed PM temperature estimation method accuracy will be validated using thermocouples, being more precise than other measurement methods such as thermal imaging. For this purpose, a wireless PM temperature measurement system, similar to the one utilized in reference [34], has been developed and implemented. Fig. 12, a photograph of the wireless PM temperature measurement system is shown, featuring the aluminum case that is attached to the rear part of the rotor. This system allows for online and accurate temperature measurements of the PMs.

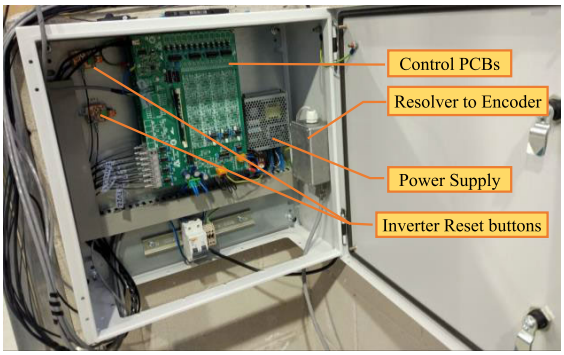

FIGURE 11. Control box with the control card and auxiliary systems.

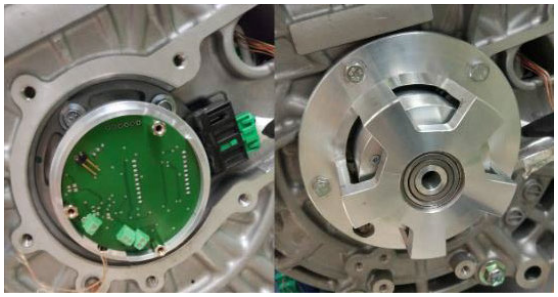

FIGURE 12. Wireless PM temperature measurement system along with the aluminum case attached to the rear part of the rotor.

B. EXPERIMENTAL RESULTS

In Fig. 13a and Fig. 13b, the measured d-axis and q-axis stator currents are displayed, analogous to Fig. 7. Furthermore, Fig. 13c and Fig. 13d depict the estimated d-axis and q-axis stator flux linkages, respectively. Notably, in Fig. 13c, the response of the stator flux to the injected quasi-square-wave current can be observed, from which the PM flux linkage is derived, as described in Section II-B. It is worth mentioning that a slight cross-coupling effect between the d-axis and q-axis can be observed in Fig. 13d.

Fig. 14 shows the d-axis DC inductance obtained by computing the mean value of dynamic inductance (9) as presented in Section II-B. The estimated PM flux linkage obtained using the method presented in Section II-B is shown in Fig. 15 for different temperatures (T_r = 20, 50, 80 and 110 °C). This data was extracted from the microcontroller, during a commissioning process. The FEA results at 20 °C are also shown in Fig. 15 for comparison. It is noticeable that the experimental results indicate a lower PM flux linkage compared to the FEA results. This difference can be attributed to a lower level of PM magnetization in the actual machine. The FEA model was not recalibrated with the experimental results. Furthermore, it should be noted that the experimental results presented in this study have been restricted to a maximum current of 450 A due to the limitations imposed by the inverter's maximum current capacity.

It can be shown from Fig. 15 that the rate of variation of PM flux linkage with PM temperature is affected by the

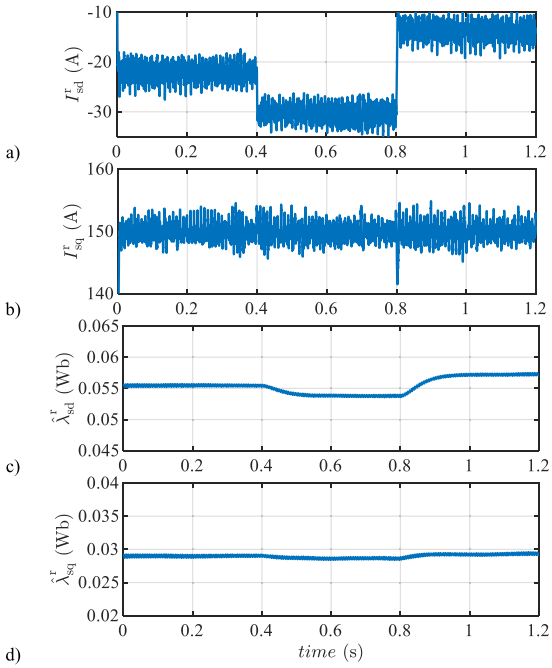

FIGURE 13. Experimental results. a) commanded d-axis current, b) commanded q-axis current, c) estimated d-axis stator flux response, d) estimated q-axis stator flux response.

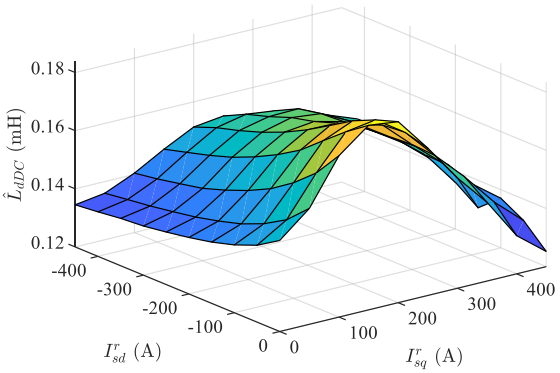

FIGURE 14. Experimental results. Estimated d-axis DC inductance. ω_r = 3000 1/min.

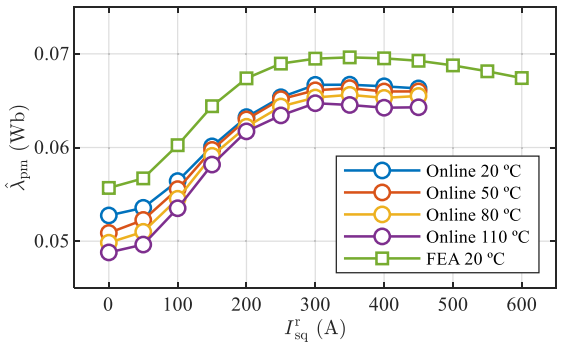

FIGURE 15. Experimental results. Estimated PM flux linkage and FEA results vs. q-axis stator current. $I^r_{sd} = -100A$, ω_r = 3000 1/min, T_r = 20, 50, 80 and 110 °C.

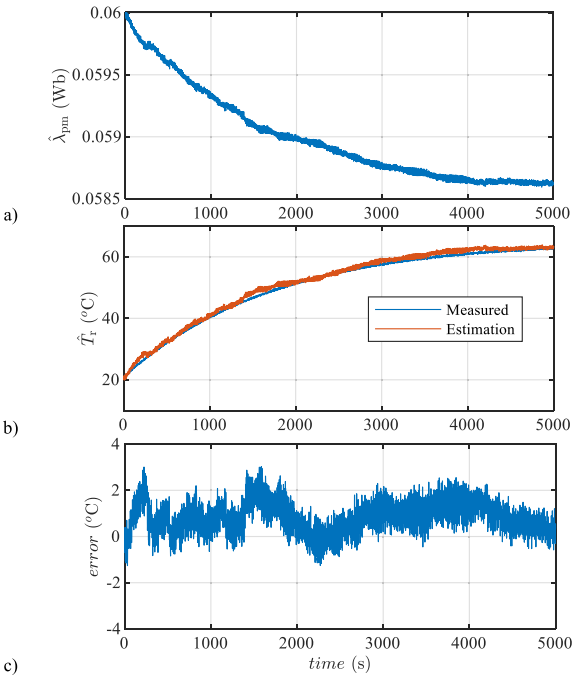

FIGURE 16. Experimental results. a) Estimated PM flux linkage, b) estimated PM temperature using LUTs and c) estimation error. $I^r_{sd} = -22A$, $I^r_{sq} = 150A$, ω_r = 3000 1/min, T = 50 Nm.

q-axis current magnitude due to the variable leakage flux property of the VLF-PMSM. The average rate of variation of PM flux linkage with PM temperature for this particular machine design is ≈ -0.6 %/°C.

A commissioning process was required to generate the complete 3D LUT in the whole current region (extending the results shown in Fig. 15) to be latter used for PM temperature estimation considering the PM flux linkage variation with stator current during machine normal operation.

The online PM temperature estimation is performed employing the LUTs and the estimated PM flux linkage, while the machine operates in a steady-state condition. Fig. 16a illustrates the estimated PM flux linkage, while Fig. 16b depicts the estimated PM temperature. Additionally, the measured PM temperature, obtained using the wireless PM temperature measurement system, is also presented in Fig. 16b. Both, measured and estimated PM temperature, are stored each second and the estimation error is calculated as the difference between estimated PM temperature and measured PM temperature for each sample. Fig. 16c displays the estimation error, which is observed to be within ±4 °C, indicating a satisfactory level of accuracy in the temperature estimation.

To validate the accuracy of the proposed method across the entire machine torque vs. speed characteristic, equivalent experiments to Fig. 16 have been conducted. These experiments aim to verify the performance and reliability of the proposed method under various torque and speed conditions. All the experiments are started at temperature of 20-30 °C, then each experiment is conducted during approximately 1.5h (around 5000 samples), reaching steady-state PM temperature for each operating point.

Considering the substantial number of operating points to be tested (several torque values, depending on the speed, each

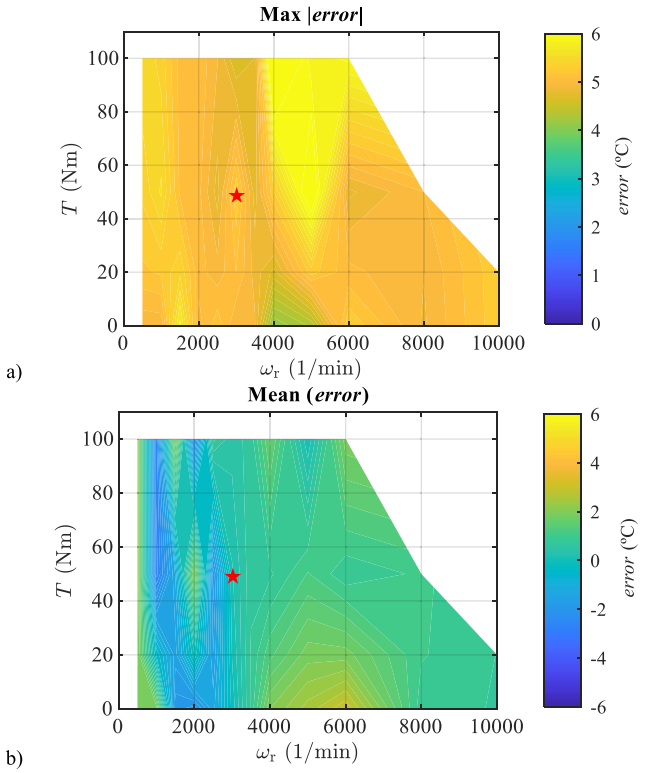

FIGURE 17. Experimental results. a) maximum absolute error during the experiments in the torque vs. speed region, and b) mean error during the experiments in the torque vs. speed region. ★: operating point shown in Fig. 16.

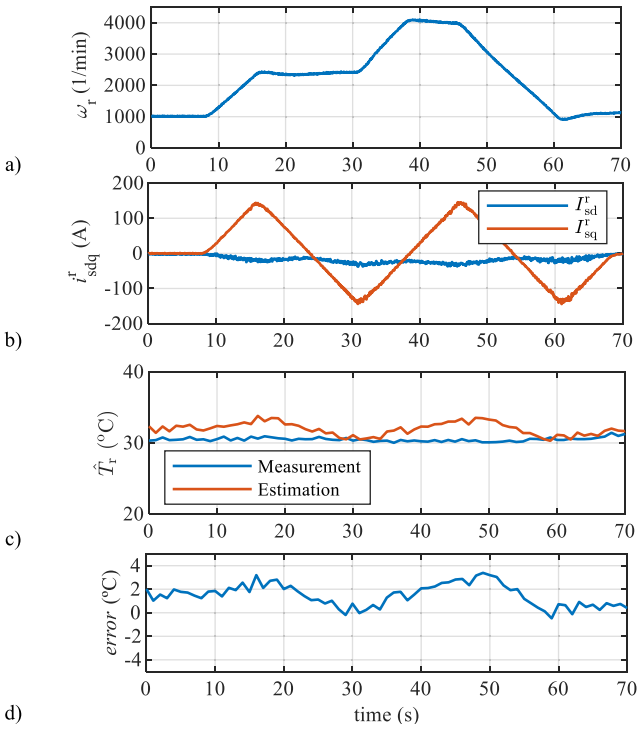

FIGURE 18. Experimental results. a) machine speed, b) d and q-axis current used during the experiment, c) estimated and measured rotor PM temperature, d) estimation error.

500 rpm) and the prolonged duration of each experiment (approximately 1.5 hours), the evaluation of the method's performance will be conducted based on the mean estimation error obtained as:

$$\text{Mean}(error) = \text{mean}(\hat{T}_r - T_r), \tag{11}$$

and the maximum absolute error obtained as:

$$\text{Max}\,|error| = \max\left(\left|\hat{T}_r - T_r\right|\right), \tag{12}$$

during the whole experiment duration; the operating point shown in Fig. 16 is marked as "⋆" in Fig. 17. A total of 65 experiments are represented in Fig. 17.

The maximum torque applied during the verification process was limited to 100 Nm due to the inverter's current capacity. The proposed method was validated for a minimum speed of 500 revolutions per minute (1/min) due to the inherent limitations of the employed flux observer (voltage model based) at low speeds.

In Fig. 17a, the absolute maximum error obtained for each operating point during the experiment is depicted. It can be observed that the maximum temperature estimation error is below 6 °C. Fig. 17b displays the mean error for each operating condition. It is shown that the mean estimation error remains within ±3 °C for the entire region.

Finally, Fig. 18 shows experimental results during load and speed transients. In the experiment shown in Fig. 18, the machine speed and currents are varied simultaneously in order to mimic the behavior in a real EV or HEV application.

In Fig. 18a, the machine speed during the experiment is shown. In Fig. 18b, the stator current of the machine is represented in the synchronous reference frame. The current follows the MTPA trajectory for both positive and negative torque. In Fig. 18c the measured and estimated PM temperature (T_r) is shown. The estimation error is finally shown in Fig. 18d. It can be observed from Fig. 18d that the proposed method provides accurate estimation under transients in torque and speed, the magnitude of the error being in any case < 3 °C. The performance of the method during standard driving cycles is out of the scope of this paper.

V. CONCLUSION

This paper introduces a novel approach for estimating the temperature of PMs in VLF-PMSMs. The method relies on the PM flux linkage variation with PM temperature considering the PM flux linkage variation with the stator current using LUTs. The consideration of PM flux linkage variation with stator current is mandatory to achieve accurate PM temperature estimation in VLF-PMSMs. The PM flux linkage is estimated from the stator flux by its response to a small-amplitude, low-frequency, quasi-square-wave current signal superimposed on the fundamental current excitation.

The proposed method achieves good accuracy from 500 rpm to 10000 rpm (95% of the total speed range); however, it cannot be used at very low or zero speed due to the diminishing magnitude of Back-EMF. Nevertheless, this

method can be combined with other estimation methods that provide accurate estimation in the low-to-zero speed region.

Simulation and experimental results are provided to demonstrate the performance of the proposed method.

REFERENCES

[1] J.-M. Kim and S.-K. Sul, "Speed control of interior permanent magnet synchronous motor drive for the flux weakening operation," *IEEE Trans. Ind. Appl.*, vol. 33, no. 1, pp. 43–48, Feb. 1997, doi: 10.1109/28.567075.

[2] V. Ostovic, "Memory motors," *IEEE Ind. Appl. Mag.*, vol. 9, no. 1, pp. 52–61, Jan. 2003, doi: 10.1109/MIA.2003.1176459.

[3] A. Athavale, T. Fukushige, T. Kato, C.-Y. Yu, and R. D. Lorenz, "Variable leakage flux IPMSMs for reduced losses over a driving cycle while maintaining suitable attributes for high-frequency injection-based rotor position self-sensing," *IEEE Trans. Ind. Appl.*, vol. 52, no. 1, pp. 234–241, Jan. 2016, doi: 10.1109/TIA.2015.2464190.

[4] B. S. Gagas, K. Sasaki, A. Athavale, T. Kato, and R. D. Lorenz, "Magnet temperature effects on the useful properties of variable flux PM synchronous machines and a mitigating method for magnetization changes," *IEEE Trans. Ind. Appl.*, vol. 53, no. 3, pp. 2189–2199, May 2017, doi: 10.1109/TIA.2017.2674627.

[5] T. Kato, T. Matsuura, K. Sasaki, and T. Tanimoto, "Principle of variable leakage flux IPMSM using arc-shaped magnet considering variable motor parameter characteristics depending on load current," in *Proc. IEEE Energy Convers. Congr. Expo.*, Oct. 2017, pp. 5803–5810.

[6] S. Li, B. Sarlioglu, S. Jurkovic, N. R. Patel, and P. Savagian, "Comparative analysis of torque compensation control algorithms of interior permanent magnet machines for automotive applications considering the effects of temperature variation," *IEEE Trans. Transport. Electrific.*, vol. 3, no. 3, pp. 668–681, Sep. 2017, doi: 10.1109/TTE.2017.2684080.

[7] A. M. El-Refaie, N. C. Harris, T. M. Jahns, and K. M. Rahman, "Thermal analysis of multibarrier interior PM synchronous machine using lumped parameter model," *IEEE Trans. Energy Convers.*, vol. 19, no. 2, pp. 303–309, Jun. 2004, doi: 10.1109/TEC.2004.827011.

[8] C. Kral, A. Haumer, and S. B. Lee, "A practical thermal model for the estimation of permanent magnet and stator winding temperatures," *IEEE Trans. Power Electron.*, vol. 29, no. 1, pp. 455–464, Jan. 2014, doi: 10.1109/TPEL.2013.2253128.

[9] D. Liang, Z. Q. Zhu, J. H. Feng, S. Y. Guo, Y. F. Li, A. F. Zhao, and J. W. Hou, "Estimation of 3-D magnet temperature distribution based on lumped-parameter and analytical hybrid thermal model for SPMSM," *IEEE Trans. Energy Convers.*, vol. 37, no. 1, pp. 515–525, Mar. 2022, doi: 10.1109/TEC.2021.3091897.

[10] D. E. G. Erazo, O. Wallscheid, and J. Böcker, "Improved fusion of permanent magnet temperature estimation techniques for synchronous motors using a Kalman filter," *IEEE Trans. Ind. Electron.*, vol. 67, no. 3, pp. 1708–1717, Mar. 2020, doi: 10.1109/TIE.2019.2905817.

[11] A. Specht, O. Wallscheid, and J. Böcker, "Determination of rotor temperature for an interior permanent magnet synchronous machine using a precise flux observer," in *Proc. Int. Power Electron. Conf.*, Hiroshima, Japan, May 2014, pp. 1501–1507, doi: 10.1109/IPEC.2014.6869784.

[12] O. Wallscheid, A. Specht, and J. Böcker, "Observing the permanent-magnet temperature of synchronous motors based on electrical fundamental wave model quantities," *IEEE Trans. Ind. Electron.*, vol. 64, no. 5, pp. 3921–3929, May 2017, doi: 10.1109/TIE.2017.2652363.

[13] G. Feng, C. Lai, J. Tjong, and N. C. Kar, "Noninvasive Kalman filter based permanent magnet temperature estimation for permanent magnet synchronous machines," *IEEE Trans. Power Electron.*, vol. 33, no. 12, pp. 10673–10682, Dec. 2018, doi: 10.1109/TPEL.2018.2808323.

[14] G. Feng, C. Lai, W. Li, M. Kelly, and N. C. Kar, "Simultaneous stator winding and permanent magnet temperature estimation for permanent magnet synchronous machines," in *Proc. 13th Int. Conf. Electr. Mach. (ICEM)*, Sep. 2018, pp. 1945–1951, doi: 10.1109/ICELMACH.2018.8506687.

[15] D. D. Reigosa, D. Fernandez, H. Yoshida, T. Kato, and F. Briz, "Permanent-magnet temperature estimation in PMSMs using pulsating high-frequency current injection," *IEEE Trans. Ind. Appl.*, vol. 51, no. 4, pp. 3159–3168, Jul. 2015, doi: 10.1109/TIA.2015.2404922.

[16] D. D. Reigosa, F. Briz, P. García, J. M. Guerrero, and M. W. Degner, "Magnet temperature estimation in surface PM machines using high-frequency signal injection," *IEEE Trans. Ind. Appl.*, vol. 46, no. 4, pp. 1468–1475, Jul. 2010, doi: 10.1109/TIA.2010.2049816.

[17] M. Ganchev, C. Kral, and T. Wolbank, "Sensorless rotor temperature estimation of permanent magnet synchronous motor under load conditions," in *Proc. 38th Annu. Conf. IEEE Ind. Electron. Soc.*, Oct. 2012, pp. 1999–2004, doi: 10.1109/IECON.2012.6388895.

[18] G. Feng, C. Lai, and N. C. Kar, "Particle-filter-based magnet flux linkage estimation for PMSM magnet condition monitoring using harmonics in machine speed," *IEEE Trans. Ind. Informat.*, vol. 13, no. 3, pp. 1280–1290, Jun. 2017, doi: 10.1109/TII.2016.2616331.

[19] G. Feng, C. Lai, J. Tjong, and N. C. Kar, "Exploring the phase angle of measured speed harmonic for efficient permanent magnet temperature estimation of PMSMs," *IEEE Trans. Energy Convers.*, vol. 34, no. 3, pp. 1475–1484, Sep. 2019, doi: 10.1109/TEC.2019.2914930.

[20] D. Fernandez, D. Reigosa, J. M. Guerrero, Z. Q. Zhu, C. Suarez, and F. Briz, "Influence of PM coating on PM magnetization state estimation methods based on magnetoresistive effect," *IEEE Trans. Ind. Appl.*, vol. 54, no. 3, pp. 2141–2150, May/Jun. 2018, doi: 10.1109/TIA.2018.2797883.

[21] S. Xiao and A. Griffo, "PWM-based flux linkage and rotor temperature estimations for permanent magnet synchronous machines," *IEEE Trans. Power Electron.*, vol. 35, no. 6, pp. 6061–6069, Jun. 2020, doi: 10.1109/TPEL.2019.2948578.

[22] D. F. Laborda, D. Díaz Reigosa, D. Fernández, K. Sasaki, T. Kato, and F. Briz, "Magnet temperature estimation in variable leakage flux permanent magnet synchronous machines using the magnet flux linkage," in *Proc. IEEE Energy Convers. Congr. Expo. (ECCE)*, Oct. 2020, pp. 6111–6117, doi: 10.1109/ECCE44975.2020.9236059.

[23] D. Reigosa, D. Fernandez, T. Tanimoto, T. Kato, and F. Briz, "Comparative analysis of BEMF and pulsating high-frequency current injection methods for PM temperature estimation in PMSMs," *IEEE Trans. Power Electron.*, vol. 32, no. 5, pp. 3691–3699, May 2017, doi: 10.1109/TPEL.2016.2592478.

[24] T. Kato, K. Sasaki, D. F. Laborda, D. F. Alonso, and D. D. Reigosa, "Magnet temperature estimation methodology by using magnet flux linkage observer for variable leakage flux IPMSM," *IEEJ Trans. Ind. Appl.*, vol. 140, no. 4, pp. 265–271, Apr. 2020, doi: 10.1541/ieejias.140.265.

[25] S. Chikazumi, *Physics of Ferromagnetism 2e* (International Series of Monographs on Physics). Oxford, U.K.: Oxford Univ. Press, 2009, pp. 118–124.

[26] P. L. Jansen and R. D. Lorenz, "A physically insightful approach to the design and accuracy assessment of flux observers for field oriented induction machine drives," *IEEE Trans. Ind. Appl.*, vol. 30, no. 1, pp. 101–110, Jan./Feb. 1994, doi: 10.1109/28.273627.

[27] J. S. Lee, C.-H. Choi, J.-K. Seok, and R. D. Lorenz, "Deadbeat-direct torque and flux control of interior permanent magnet synchronous machines with discrete time stator current and stator flux linkage observer," *IEEE Trans. Ind. Appl.*, vol. 47, no. 4, pp. 1749–1758, Jul./Aug. 2011, doi: 10.1109/TIA.2011.2154293.

[28] H. Rehman, A. Derdiyok, M. K. Guven, and L. Xu, "A new current model flux observer for wide speed range sensorless control of an induction machine," *IEEE Trans. Power Electron.*, vol. 17, no. 6, pp. 1041–1048, Nov. 2002, doi: 10.1109/TPEL.2002.805579.

[29] K. D. Hurst, T. G. Habetler, G. Griva, and F. Profumo, "Zero-speed tacholess IM torque control: Simply a matter of stator voltage integration," *IEEE Trans. Ind. Appl.*, vol. 34, no. 4, pp. 790–795, Jul./Aug. 1998, doi: 10.1109/28.703975.

[30] D. G. Holmes and T. A. Lipo, *Pulse Width Modulation for Power Converters: Principles and Practice*. New York, NY, USA: Wiley, 2003, pp. 612–620.

[31] M. Hinkkanen and J. Luomi, "Modified integrator for voltage model flux estimation of induction motors," *IEEE Trans. Ind. Electron.*, vol. 50, no. 4, pp. 818–820, Aug. 2003, doi: 10.1109/TIE.2003.814996.

[32] B. Shuang and Z.-Q. Zhu, "A novel method for estimating the high frequency incremental DQ-axis and cross-coupling inductances in interior permanent magnet synchronous machines," *IEEE Trans. Ind. Appl.*, vol. 57, no. 5, pp. 4913–4923, Sep. 2021, doi: 10.1109/TIA.2021.3089444.

[33] M. Martinez, D. F. Laborda, D. Reigosa, D. Fernandez, J. M. Guerrero, and F. Briz, "SynRM sensorless torque estimation using high-frequency signal injection," *IEEE Trans. Ind. Appl.*, vol. 57, no. 6, pp. 6083–6092, Nov./Dec. 2021, doi: 10.1109/TIA.2021.3111840.

[34] D. Reigosa, D. Fernández, M. Martínez, J. M. Guerrero, A. B. Diez, and F. Briz, "Magnet temperature estimation in permanent magnet synchronous machines using the high frequency inductance," *IEEE Trans. Ind. Appl.*, vol. 55, no. 3, pp. 2750–2757, May/Jun. 2019, doi: 10.1109/TIA.2019.2895557.

DIEGO F. LABORDA (Member, IEEE) received the B.S. degree in industrial electronic engineering, the M.S. degree in electric energy conversion and power electronics engineering, and the Ph.D. degree in electrical engineering from the University of Oviedo, Gijón, Spain, in 2016, 2018, and 2022, respectively. Since 2018, he has been a Researcher with the Department of Electrical, Computer and Systems Engineering, University of Oviedo. His research interests include electric machines and power electronics for electric vehicles, wireless measurement systems, and digital signal processing.

DAVID REIGOSA (Senior Member, IEEE) was born in Spain, in 1979. He received the M.E. and Ph.D. degrees in electrical engineering from the University of Oviedo, Spain, in 2003 and 2007, respectively. He is currently a Full Professor with the Department of Electrical Engineering, University of Oviedo. He was a Visitor Scholar with the Wisconsin Electric Machines and Power Electronics Consortium, University of Wisconsin, Madison, in 2007. He was also a Visitor Professor with the Electrical Machines and Drives Group, University of Sheffield, U.K., in 2016. His research interests include sensorless control of induction motors, permanent magnet synchronous motors, and digital signal processing. He was a recipient of nine IEEE Industry Applications Society Conference and IEEE Energy Conversion Congress and Exposition prize paper awards. From 2004 to 2008, he was awarded and fellowship in the Personnel Research Training Program funded by the Regional Ministry of Education and Science of the Principality of Asturias.

DANIEL FERNÁNDEZ (Member, IEEE) received the M.S. degree in power electronic engineering and the Ph.D. degree in electrical engineering from the University of Oviedo, Spain, in 2013 and 2017, respectively.

He was an Intern with the Nissan Advanced Technology Center, Japan, in 2013, a Visiting Student with the University of Sheffield, in 2015, and a Visiting Professor with the University of Padova, in 2019. He is currently an Associate Professor with the University of Oviedo. His research interests include design, control, and diagnostics of electric machines and drives. He was awarded a fellowship in the Personnel Research Training Program funded by the Regional Ministry of Education and Science of the Principality of Asturias, in 2013. He was a recipient of the University of Oviedo Outstanding Ph.D. Thesis Award, in 2018, and four IEEE Industry Applications Society Conference prize paper awards.

KENSUKE SASAKI received the B.S. and M.S. degrees in electrical engineering from Yokohama National University, Yokohama, Japan, in 2003 and 2005, respectively.

In 2005, he joined the Nissan Research Center, Atsugi, Japan, where he contributed to inverter circuit design, converter circuit design, and control. From 2014 to 2016, he was a Visiting Engineer with the Wisconsin Electric Machines and Power Electronics Consortium (WEMPEC), University of Wisconsin–Madison, Madison, WI, USA. He is currently with the Electric Vehicle System Laboratory, Nissan Motor Company Ltd., Atsugi. His research interest includes electric motor design and control.

Mr. Sasaki is a member of the Institute of Electrical Engineers of Japan.

TAKASHI KATO (Member, IEEE) received the B.S. degree in mechanical system engineering from Kansai University, Osaka, Japan, in 1997, and the Ph.D. degree from the Shibaura Institute of Technology, Tokyo, Japan, in 2015. He joined Nissan Motor Company Ltd., in 1997, and the Nissan Research Center, in 2001. He has contributed to the electric machine design and control. He was a Visiting Researcher with the Wisconsin Electric Machines and Power Electronics Consortium (WEMPEC), University of Wisconsin–Madison, from 2010 to 2012. His research interests include electric motor design, control, power electronics devices, and electric vehicle systems. He is currently the Deputy General Manager of the EV System Laboratory, Nissan Research Division. He is a Senior Member of the Institute of Electrical Engineers of Japan (IEEJ) and a member of the Society of Automotive Engineers of Japan (JSAE) and the Japan Society of Mechanical Engineers (JSME).

FERNANDO BRIZ (Senior Member, IEEE) received the M.S. and Ph.D. degrees from the University of Oviedo, Gijón, Spain, in 1990 and 1996, respectively.

He is currently a Full Professor with the Department of Electrical, Computer and Systems Engineering, University of Oviedo. His research interests include electronic power converters and ac drives, power systems, machine monitoring and diagnostics, and digital signal processing.

Dr. Briz is a member of the Executive Board of ECCE. He was a recipient of the IEEE TRANSACTIONS ON INDUSTRY APPLICATIONS Award and the nine IEEE Industry Applications Society Conference and the IEEE Energy Conversion Congress and Exposition Prize Paper Awards. He is the Chair of the Industrial Power Conversion System Department (IPCSD) of the IAS. He is the Past Chair of the Industrial Drives Committee of IPCSD. He has served on scientific committees and as the Vice Chair or the Technical Program Chair for several conferences, including ECCE, IEMDC, ICEM, ICEMS, and SLED. He is the Deputy Editor-in-Chief and a member of the Steering Committee of IEEE JOURNAL OF EMERGING AND SELECTED TOPICS IN POWER ELECTRONICS. He is an Associate Editor of IEEE TRANSACTIONS ON INDUSTRY APPLICATIONS.